Contents lists available at ScienceDirect

Arabian Journal of Chemistry

journal homepage: www.ksu.edu.sa

Original article

Preparation and utilization of Zn-La oxide nanocatalyst as a binary composite for photocatalytic degradation of methylene blue dye: Optimization through RSM-BBD

Basir Maleki [a], Tahseen Hameed Khlaif [b], Majeed Khudhair Jasim [a], Mohsen Mansouri [a,*]

[a] Department of Chemical Engineering, Ilam University, Ilam, Iran
[b] Department of Petroleum Engineering, University of Kerbala, Karbala, Iraq

ARTICLE INFO

Keywords:
Photocatalytic
Zn-La oxide nanocatalyst
Methylene blue
Response surface methodology
Kinetic

ABSTRACT

In this research, the photocatalytic degradation of methylene blue (MB) dye was explored by employing Zn-La (zinc-lanthanum) oxide nanocatalysts under UV irradiation. Preparation of Zn-La oxide nanocatalysts was executed utilizing the co-precipitation technique, and the surface and morphology of the fabricated nanocatalyst were examined via X-Ray diffraction analysis (XRD), Fourier-transform infrared spectroscopy (FTIR), Brunauer-Emmett-Teller (BET), Barrett-Joyner-Halenda (BJH), Field emission scanning electron microscopy (FESEM), Transmission electron microscopy (TEM), and energy dispersive X-ray (EDX) methods. BET-BJH analysis demonstrated that the specific surface area of the Zn-La oxide nanocatalyst was 20.43 m^2/g. Moreover, the response surface methodology (RSM) procedure was utilized to influence the operational factors i.e., catalyst amount, pH, H_2O_2 dose, and UV power. The quadratic model proposed via the RSM technique with a high R^2 value of 0.89, demonstrates its reliability. Besides, the maximum percentage of MB dye removal reached 75.18% under optimal conditions, which include a catalyst amount of 12.05 mg, pH of 9, H_2O_2 dose of 0.44 mL, UV power of 23 W, and a reaction time of 45 min. Further, under the mentioned conditions, after 120 min, the MB degradation efficiency reached 98.8%. The kinetic study exhibited that the reaction rate constant was 0.0363 min^{-1}. According to the outcomes, Zn-La oxides have a higher ability to remove MB. After 5 consecutive reuse rounds, the reduction in the yield of MB removal using Zn-La oxide nanocatalysts was 5.4%. This study demonstrates that the Zn-La oxide nanocatalyst can be promisingly utilized for the degradation of MB dye suspension solution.

1. Introduction

The issue of pollution has emerged as one of the most severe problems demanding immediate attention and remediation. Instances of environmental contamination include water pollution, stemming from the discharge of waste from factories, petroleum refining processes, and households (Pinchujit et al., 2022; Phuruangrat et al., 2023). Presently, the annual production of over 100,000 different types of dyes amounts to approximately 7×10^5 tons (Phuruangrat et al., 2023). The textile industry, being the primary consumer, utilizes around 36,000 tons of dyes annually, with nearly 20% of them being discarded as waste in the form of textile effluents (Norabadi et al., 2020). Water contamination stands out as a critical aspect of environmental pollution, primarily attributed to harmful chemicals and organic dyes present in industrial wastewater (Yayapao et al., 2015). such organic dyes in waste effluents is of great environmental importance due to their non-biodegradability, high toxicity to aquatic organisms, and carcinogenic effects on humans (Vasiljevic et al., 2020). Industrial establishments utilize a large quantity of water, and then they produce a lot of wastewater, which consists of a diverse range of hazardous pollutants in different concentrations (Fathirad et al., 2021). Industrial wastewater effluents pose a significant threat to human health due to their elevated levels of hazardous and toxic substances. Consequently, it is imperative to treat these effluents to eliminate the presence of harmful pollutants before their discharge into water bodies (Etemadi et al., 2021).

Physical treatments are considered one of the promising alternatives such as flocculation, activated coal adsorption, and reverse osmosis are non-destructive and fundamentally transfer contaminants to other

* Corresponding author.
E-mail address: mansouri2010@yahoo.com (M. Mansouri).

https://doi.org/10.1016/j.arabjc.2024.105667
Received 19 November 2023; Accepted 5 February 2024
Available online 12 February 2024

media, leading to secondary pollution (Mangeli et al., 2021; Maleki and Esmaeili 2023a). Photocatalysis involving heterogeneous semiconductors has been extensively investigated and has proven to be an effective strategy for the degradation of numerous organic contaminants. Additionally, this approach is economically feasible (Abbasi 2023). Photocatalysis has a high potential in terms of cleaning up the environment and using renewable energy. Semiconductor-based photocatalysis has been extensively explored for environmental fields and has proven to be a cleaning technology (Chen et al., 2016).

Heterogeneous photocatalysis holds significant practical value as it demonstrates the capability to achieve almost complete mineralization of a broad range of toxic organic substances (Maleki et al., 2022). Consequently, it may be useful to use this technique for treating polluted water to get rid of many contaminants (Abbasi et al., 2019). it is well known, that, photocatalysis generally involves a series of light-induced redox processes in which the light plays a major role. They occur when a suitable semiconductor nanoparticle is exposed to light which has energy huger than the band gap (Nazari et al., 2023). Photocatalytic treatment is considered one of the most effective ways for removing contaminants from aqueous media owing to various advantages. These include high degradation efficiency leading to the production of CO_2 and H_2O, an exceptionally rapid degradation rate, and the generation of other elements as end products (Afmataj et al., 2023). The electron-hole pairs produced through photoproduction are the basis of photocatalytic processes (Ashrafi et al., 2021). The electron-hole pairs serve as carriers where oxidation/reduction processes occur at the semiconductor surface. Consequently, radical species are generated, interacting with organic contaminants and facilitating the decomposition of contamination and subsequent mineralization (Hossein Panahi et al., 2020).

The utilization of semiconductors in the photocatalytic process has been explored, proving to be a highly efficient and environmentally friendly technique for pollutant degradation (Khan et al., 2022). Semiconductors with a broad band gap, such as ZnO, are particularly significant as photocatalysts (Abbasi et al., 2020). Zinc oxides are of great interest due to their ready availability, relatively low cost, good stability, low toxicity, and exceptional potential to generate highly oxidizing radical species (Afmataj et al., 2023). Moreover, these semiconductors show a promising future for manufacturing highly sensitive solar cells to dye, and for the remediation of harmful organic components by photocatalytic therapy (Lin et al., 2018). The doping methodology proves to be a powerful and reliable approach to modify the properties of both structural and catalytic semiconductor oxides (Chen et al., 2016). The introduction of a dopant metal is typically designed to enable a response to visible light, facilitating the formation of hybrid energy levels between the conduction band and the valence band (VB) of these oxides (Van et al., 2022). Hence, appropriate doping can inhibit the recombination of photoinduced electron–hole pair (e^-/h^+) and improve the semiconductor oxides' photoactivity (Elfeky et al., 2020). The semiconductor photoactivity may be developed by means of doping techniques through the use of various sets of elements, like the following types of metals (Au, Ag, Cu, Co, etc.) (Ruzimuradov et al., 2017), nonmetals (Mg, C, N, S, etc.) (Chaker et al., 2021), and rare soil metals (Ce, La, Eu, etc.) (Mazierski et al., 2017). Lanthanide ions, categorized as rare earth metals, are deemed promising for doping. With their 4f electron configuration, these ions can effectively serve as a source of electrons, restricting them in the conduction band (CB) of the photocatalyst (Jian et al., 2022). Besides that, doping by using lanthanide elements could improve the sensitivity of light and accelerate the diffusion and transport of reactive particles and products by raising the adsorption capability of the adsorbate (Shwetharani et al., 2018).

Numerous experimental and theoretical studies have elucidated that the optical properties and electronic characteristics of substances can be enhanced through the incorporation of dopant ions from rare earth metals (Yan et al., 2022). Lanthanum ions, in particular, are noteworthy for their electron-trapping effect facilitated by the adaptive sites of chemical valence (La^{2+} and La^{3+}). Lanthanum (La) is recognized as one of the rare earth metal elements abundant in soil. Its outstanding properties and widespread availability have led to extensive research for various purposes (Song et al., 2021). Lanthanum is classified as an effective dopant element capable of modifying the band structure and improving the photocatalytic properties of different semiconductor oxides (Hajiali et al., 2021). Some authors show that the La-doped semiconductor has perfectly different chemical–physical properties compared with those of the undoped semiconductor (Song et al., 2021). The existence of La in the ZnO lattice produces electron capture and thus prevents the hole recombination for limiting the electron–hole pairs (e^-/h^+) formation, which then improves the semiconductor photochemical efficiency (Kraidi et al., 2023). Additionally, the presence of lanthanum in the zinc oxide (ZnO) lattice reduces its band gap, altering its optical behavior towards the visible region. This enhancement in the photoactivity of the semiconductor is particularly beneficial in the presence of sunlight (Liang and Esmaeili, 2021). Chaker et al. 2021, doped lanthanum onto titanium oxide and employed an aqueous solution for the removal of methyl orange, achieving a remarkable 99.89% removal under optimal conditions. Mazierski et al. 2017 scrutinized the removal of toluene using lanthanide-TiO_2 nanocatalysts. The findings revealed a 30% removal after 60 min.

The main objective of this study is to investigate a strong and highly active photocatalyst in methylene blue dye degradation from aqueous suspension. Through an examination of previous papers on the removal of MB, it becomes evident that various catalysts are frequently employed. Consequently, there is a significant gap in this area. To the best of our knowledge, this research paper represents the first endeavor to address the removal of MB from aqueous suspension using Zn-La oxide nanocatalysts. To achieve this goal, Zn-La oxide nanoparticles were synthesized and utilized. Structural characteristics of these nanoparticles were elucidated through diverse analyses, including FESEM, EDX, XRD, TEM, BET, and FTIR. Furthermore, the study investigated the influence of key variables such as catalyst dosage, pH, UV irradiation intensity, and the addition of H_2O_2 on the degradation efficiency of MB dye. Optimization was performed using the RSM-BBD statistical technique. Additionally, reliability assessments of the photocatalyst and kinetic studies were conducted to evaluate the economic feasibility of the procedure.

2. Materials and methods

2.1. Chemicals and devices

Several chemicals were employed in this study, such as Zn $(NO_3)_2{\cdot}6H_2O$ (>99%), La $(NO_3)_3{\cdot}6H_2O$ (>99%), Na_2CO_3 (>99.9%), NaOH (>99%), Hydrogen peroxide, Hydrochloric acid (>98%), and Methylene blue ($C_{16}H_{18}N_3SCl$). These chemicals were bought from Merck company with high purities. Besides, the physical characteristics and molecular structure of MB utilized in this research are presented in Table 1 and Fig. 1, respectively.

Table 1
Physical characteristics and molecular structure of MB.

Common name	Methylene blue
C.I. Number	52015
Color	Blue
Solubility aqueous	3,55%
Empirical formula	C_{16} H_{18} N_3 S Cl
Melting point	100–110 °C
Molecular weight	319.85 g/mol
Molecular volume	241.9 cm^3/mol
Molecular diameter	0.80 nm

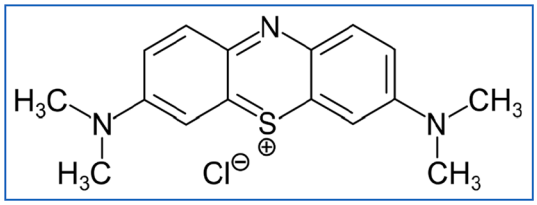

Fig. 1. Methylene blue structure.

2.2. Catalyst fabrication procedure

2.2.1. ZnO synthesis

One of the most important ways to synthesize Zinc oxide nano-sized particles chemically is a co-precipitation technique (Kraidi et al., 2023; Maleki and Ashraf Talesh, 2021). briefly, precursor solution including 0.5 M (14.9 gm) of Zn $(NO_3)_2{\cdot}6H_2O$ was dissolved in (100 mL) of deionized distilled water. In order to make ZnO sol, 1 M (53 mg) Na_2CO_3 was added (75) ml into the solution of Zinc nitrate hexahydrate dropwise under constant stirring for two hours at 70 °C. Then, the precipitate was filtered and, right after that washed many times with deionized water to remove impurities. Afterward, ZnO nanoparticles were dried by heating up to 80 °C using an oven for 10 h to eliminate water molecules, and finally, nanoparticles were calcined utilizing an air furnace at 400 °C for two h to improve their crystallinity.

2.2.2. Zn-Laoxide nanocatalyst synthesis

Zn-La oxide nanoparticles (Zn-La oxide) were developed by dissolving (10.8 gm) of La $(NO_3)_3{\cdot}6H_2O$ and (14.9 g) zinc nitrate hexahydrate in 100 mL deionized distilled water separately (Jian et al., 2022). At 70 °C, after that (80 mL) sodium carbonate was added to the solution and continuously stirred for 2 h. The resulting mix was stirred by magnet-stirrer for 1 h. Afterwards, the mix was washed 3 times with water and ethanol, and then dried at 100 °C for 8 h. Finally, the powder obtained from the suspension was subjected to calcination at 600 °C for a duration of 4 h to obtain Zn-La oxide nanoparticles.

2.2.3. Zn-La oxide nanocatalyst characterization

To find out the photocatalyst properties, in this part of the study, the crystal structure of ZnOnano-sized particles was investigated utilizing X-ray diffraction (XRD) techniques, using a type of Philips PW1820 diffractometer equipped with Cu Kα radiation. In addition, with a range of 400 to 4000 cm^{-1}, a VERTEX70 FTIR device was employed to collect infrared spectra. Besides, a Quanta 200 SEM device with an EDX apparatus was employed to examine the morphology, surface composition, and grain size. From the adsorption–desorption processes, the BET surface area of the Zn-La oxide nanocatalyst was characterized using a Jasco V-670 spectrophotometer setting at ambient temperature.

2.3. Photocatalytic procedure

The experiment of removing MB dye from the solution was done using: an LED as a source of light irradiation with wavelength 600 nm, nanocatalyst (50–50 Zn-La oxide), 20 mL MB solution with concentration 5 ppm, at ambient temperature (25–30 °C). On the other hand, the experiment was performed under various conditions: UV irradiation intensity, pH of the solution, the dosage of nanocatalyst, and amount of added scavenger (H_2O_2) in order to study the effect of these parameters on the MB removing process. Nevertheless, the above four independent variables were controlled by employing the determined values as follows: pH of solution (3, 6, 9), catalyst loading (4, 12, 20 wt%) mg, scavenger adding (H_2O_2: 0.2, 0.5, 0.8 mL), applied UV lamp power (8, 15, 23 W).H_2O_2 plays a crucial role in the photocatalytic degradation process. The addition of a specific amount of H_2O_2 has a beneficial impact on the photocatalytic degradation process. This is attributed to its ability to reduce the rate of formation of photogenerated electron-hole pairs, thereby diminishing the prolonged exposure time required for the process (Kraidi et al., 2023). Moreover, to determine MB concentration a UV-spectrophotometer at wavelength 600 nm and determination of MB degradation employed the following equation (1) (Liang and Esmaeili, 2021):

$$\%MBRemoval = \frac{C_0 - C_t}{C_0} * 100\% \quad (1)$$

where C_0 is the MB initial concentration at time = 0 and C_t is the MB concentration at time = t.

2.4. RSM-BBD procedure

For optimizing influential variables on MB dye efficiency, BBD utilizing Design Expert Software was employed. In this regard, the impact of four parameters on three levels was utilized. Table 2 demonstrates a matrix of the photocatalytic parameters of the tests. Additionally, a 2nd-order polynomial relationship, based on equation (2), was employed for predicting the relationship between key factors and MB dye efficiency (Maleki et al., 2023a; Maleki et al., 2023b).

$$MBdegradation(\%) = b_0 + \sum_{i=1}^{k} b_i Z_i + \sum_{i-1}^{k} b_{ii} Z_i^2 + \sum_{i=1}^{k} \sum_{j=i+1}^{k} b_{ij} Z_i Z_j + \varepsilon \quad (2)$$

Here, Zi and Zj are reaction variables (i.e., pH of solution, catalyst loading, UV lamp power,and MB concentration,). Besides, b_0 and ε are a constant amount and the unanticipated error, respectively. Additionally, bi, bii, and bij illustrate reaction constants.According to the RSM-BBD approach, the number of trials (runs) also depends on the number of independent variables and the number of values for each variable. Here in this research, has four parameters with three values (high, intermediate, low) for each variable (Maleki et al., 2024a).

3. Results and discussion

3.1. Photocatalyst analysis

The powder XRD technique was used to recognize the La-doped ZnO crystal structure, size, and lattice nature. Fig. 2 offers the XRD pattern for pure ZnO and Zn-La oxide nanoparticles which were developed by co-precipitated techniques. According to the JCPDS card no: 79-0208, the diffraction peaks of pure ZnO were at: 31.67°, 34.41°, 47.64°, 56.62°, 62.87°, 67.86°, and 69.10° matches with the (100), (002), (101), (102), (110), (103), (112), and (201) planes of hexagonal structure of (ZnO) (Maleki et al., 2023b). In spite of, the Zn-La oxide has the positions of the same peaks and almost the same intensity as that of pure ZnO, but it is clear that there are a new peaks at the positions (25.3, 26.4, 31.9, 34.5, 36.3, 38.3, 39.6, 42.2, 44, 47.6, 50.5, 52.7, 59.7, 63.2, 67.5) conforms with the intensities (which be compatible with the lattice planes of) (564, 369, 631, 830, 632, 688, 670, 659, 603, 519, 530, 379, 452, 338) respectively. These new peaks are related to the lanthanum oxides (La_2O_3) according to the JCPDS card no: 83-1355. This is due to the large difference between the ionic radii of Zn^{+2} ion (0.75 A°) and La^{+3} ion (1.15 A°) (Maleki and Esmaeili, 2023b). Furthermore, In the XRD peaks of the (Zn-La oxide) samples, notice the peaks broadened markedly, and reflection developed at many new

Table 2
The experimental design implemented by Design Expert Software.

Factors	Symbol	Ranges
Catalyst amount (mg)	A	4–20
pH	B	3–9
H_2O_2 dose (mL)	C	0.2–0.8
UV- powe	D	8–23

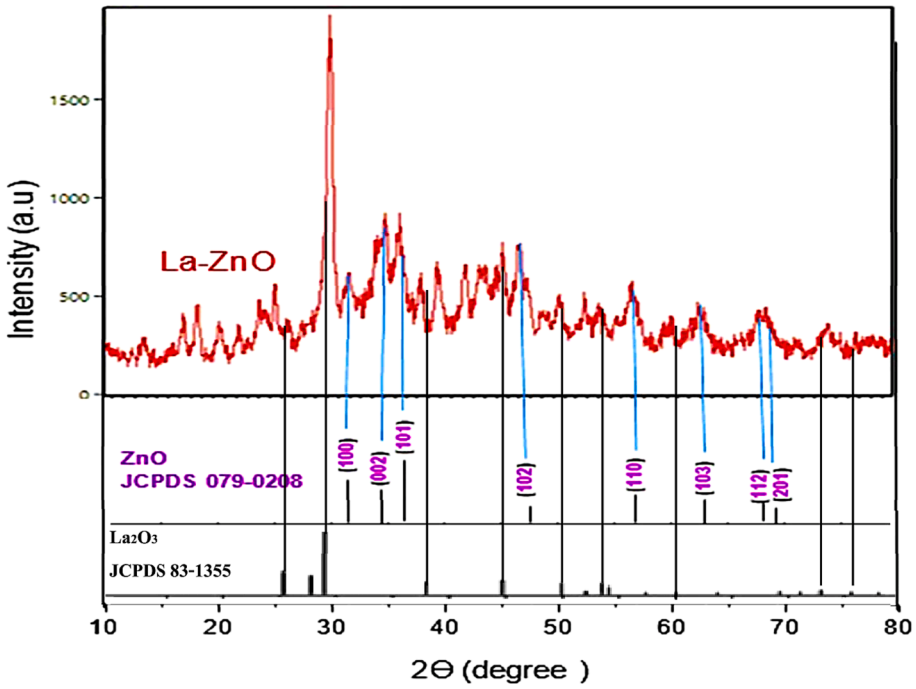

Fig. 2. XRD pattern pure ZnO and Zn-La oxide nanoparticles.

positions (2 theta) indicates the existence of lanthanum oxides as a new phase (Mohamed et al., 2022). Moreover, the peaks shifted noticeably to shorter diffraction angles could reveal a lattice expansion, suggesting that La ions, which are remarkedly larger than Zn ions, entered the ZnO lattice as substitutes (Murshed et al., 2022). On the other hand, these many new peaks also suggest that there are big changes in the crystal structure return to the La loading. However, it can be noted that the Zn-La oxide nano-samples have wider diffraction peaks and lower intensity than pure ZnO. A simple comparison will be done between diffraction peaks at (1 0 0), (0 0 2), and (1 0 1) planes (in the range of $2\theta = 30–40$) of both pure and Zn-La oxide demonstrated in Fig. 2. The peak position of Zn-La oxide, in relation to its position in pure ZnO, exhibited a slight shift to a lower angle with minimal change in the peak position. This peak shifting of XRD lines based on the doping process strongly proves that La^{+3} was related to the ZnO lattice (Noorimotlagh et al., 2020). Generally, these results indicate that there is bonding between

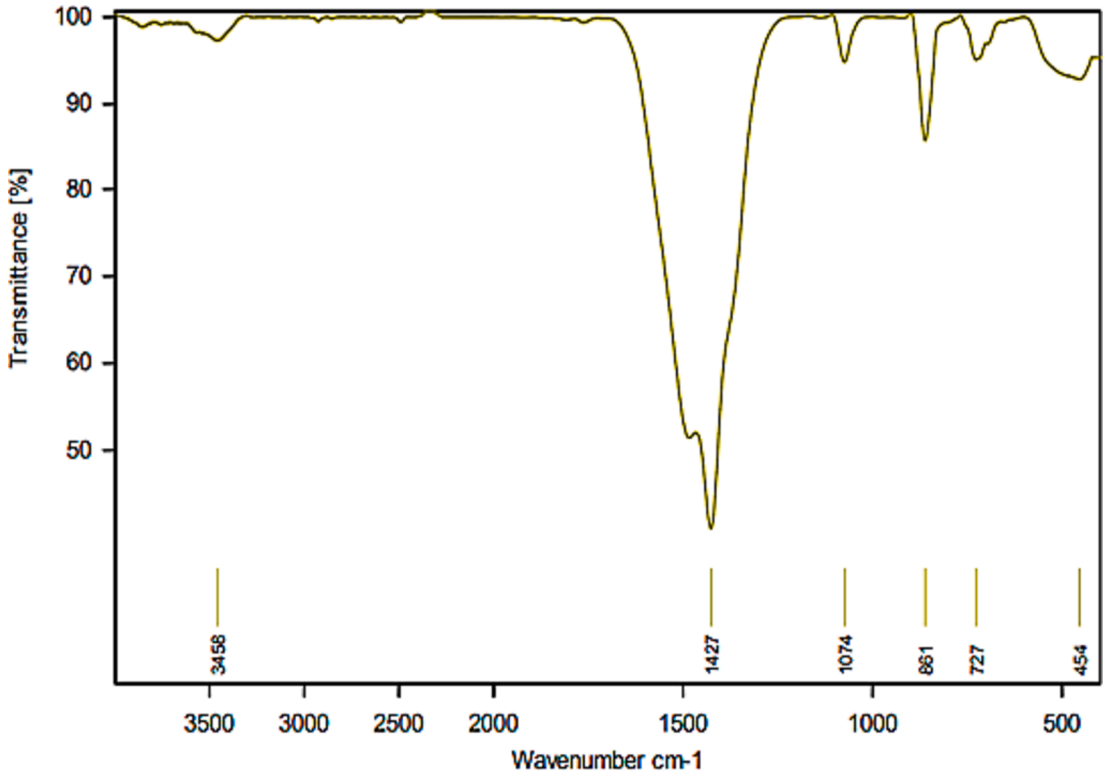

Fig. 3. FTIR spectrum Zn-La oxides nanoparticles.

lanthanum and zinc oxide, and the interaction between lanthanum oxide clusters and the ZnO surface is significantly developed (Law et al., 2021).

In order to study closely vibrational mode of the Zn-La oxide nanoparticles closely, FTIR spectra were employed, which accurately detail functional groups within the sample. The FTIR spectra of Zn-La oxide nanoparticles as a catalyst were taken in the wavenumber range of (400–4000) cm^{-1} as shown in Fig. 3. The FT-IR pattern of Zn-La oxide nanoparticles illustrated well-defined absorption peaks at (454, 727, 861, 1074, 1427, 3458) cm^{-1}. The broad absorption band observed at 454 cm^{-1} gives an indicator of the existence of stretching vibrational modes of Zn–O (Anandan et al., 2007). Moreover, the wide absorption band at 454 cm^{-1} may be the characteristic absorption of the Zn–O bond stretching vibration of ZnO crystal wurtzite hexagonal type. The peak appearing at 727 cm^{-1} is attributed to the stretching vibrational modes of La–Zn–O (Anandan et al., 2007). However, the stretching vibration of the La-O bond band might appear at 727 cm^{-1} wavelengths (Thi and Lee, 2017). The sharp peak at 861 cm^{-1} revealed the existence of bending vibration modes of the Zn–O bond. A sharp absorption signal occurred at 1074 cm^{-1} is assigned to the cyclic –C–C stretching vibration (Ramírez-Aparicio et al., 2021). Evidently, the broad characteristic absorption peak centered at 1427 cm^{-1} is likely associated with the organic pollutants, particularly the C═O and C–O bonding [43].The broad absorption bands at 3458 cm^{-1} are assigned to the stretching vibration of O–H species that are formed via dissociative adsorption of H_2O molecule (Thi and Lee, 2017).

The morphology of the synthesized nanoparticles was scrutinized through FESEM as demonstrated in Fig. 4. The presence of a dopant in the nanoparticles of the catalyst (Zn-La oxide) was discovered by FESEM, in which dopant surface morphology was studied. The FESEM micrograph of the sample revealed that these nanoparticles are generally spherical in shape as clearly shown in Fig. 4. However, the Zn-La oxide nanoparticles exhibit a consistent and uniform morphology, with particle sizes ranging between 20 and 40 nm. It is evident that the La doping diffuses uniformly and homogeneously into various sites, explaining the slight reduction in the sizes of doped nanoparticles. Additionally, it is evident that these nanoparticles have relatively low porosity in the background.

Energy Dispersive X-ray (EDX) analysis was done to prove both the presence of La on the surface of catalyst ZnO nanoparticles (Zn-La oxide) and to confirm the absence of any impurity phase or elements (see Fig. 5). Moreover, it is used to determine the elemental compositions of the prepared nanocatalyst (Zn-La oxide). The result of EDX spectra as revealed in Fig. 5 corresponds with the XRD results, revealing that the nano-catalyst particles consist of three elements La, Zn, and O. with weight ratios of 48.80, 28.31, and 22.89 respectively, and Consequently, it also confirms the existence of La in ZnO. The deposition of gold film over the sample resulted in the detection of an Au core.

The physical properties of the synthesized nanocatalyst (Zn-La oxide) were assessed using both BET and BJH methods, employing the N_2 adsorption–desorption isotherm environment, as depicted in Fig. 6. BET surface area was found to be 20.4 m^2/g and the pore volume was 4.6 cm^3/g. The Zn-La oxidecatalyst has a Type IV isotherm with a typical H3 hysteresis loop, according to the IUPAC classification. BET isotherms can be described as follows (Anandan et al., 2007; Thi and Lee, 2017):

I) Type (a): Reversible isotherm typical for microporous solids with narrow micropores (<≈1 nm). Type (b): Similar to (c) but for solids containing both wider micropores and narrow mesopores (<≈2.5 nm). II) Reversible Type II: Corresponds to nonporous or macroporous materials. Point B indicates monolayer coverage and a sharp curvature change signals the beginning of multilayer adsorption. III) Type III: Obtained when interactions between adsorbent and adsorbate are weak, providing limited information about monolayer coverage.

IV) Type IV(a): Two patterns related to the width of pores. Obtained for materials with wider pores above the critical width, especially common in mesoporous materials. Type IV(b): Observed for materials with mesopores of smaller widths. V) Type V: Shape similar to Type III at low P/P0, attributed to weak adsorbent–adsorbate interactions. Hysteresis at higher pressures, resembling Type IV(a), indicates molecular clustering followed by pore filling. VI) Type VI: Typical for multilayer adsorption on materials with highly uniform nonporous surfaces. The isotherm appears as a stepwise curve, dependent on material, gas, and temperature (Thi and Lee, 2017; Ramírez-Aparicio et al., 2021).

Hence, in Fig. 6(a), the N_2 adsorption–desorption isotherm illustrates that a rapid development of the hysteresis loop $P/P_0 > 0.8$ confirming the accumulation of pores. According to the findings acquired from (BJH) Analysis, as in Fig. 4b, which indicates a pore size of 14.1 nm, it can be deduced that the prepared catalyst is a mesoporous material. Besides, the numerical values of BET analysis are presented in Table 3.

The high-resolution transmission electron microscope (TEM) image of Zn-La oxides nanocatalyst demonstrates that includes an average diameter of 20–30 nm and is amorphous (Fig. 7). The high surface area and small particle size of the Zn-La oxides nanocatalyst may furnish great active sites and pores for catalysis and provide a higher MB degradation. Furthermore, amorphous catalysts exhibit a more flexible composition, a disordered atomic structure, and an increased number of

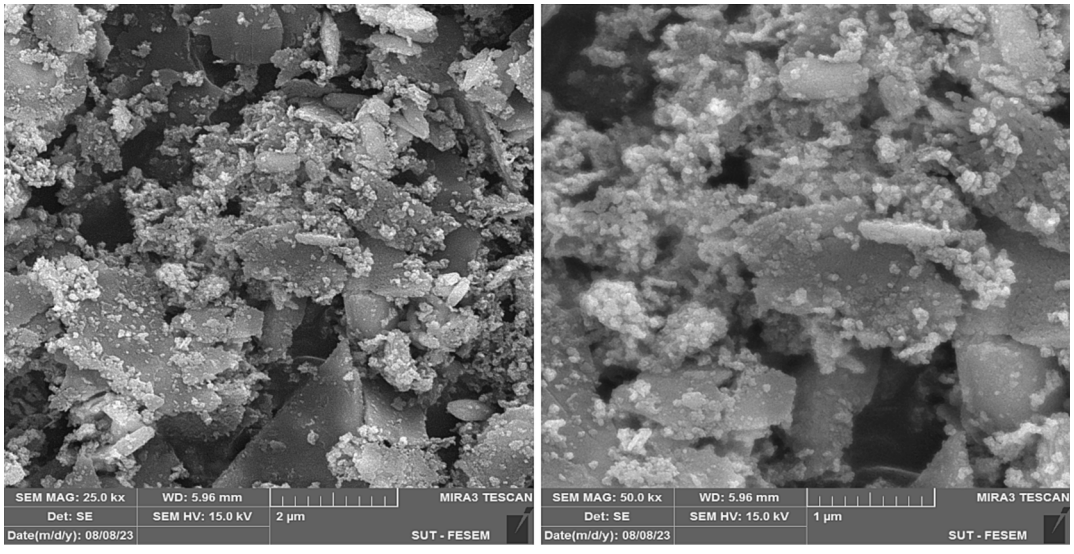

Fig. 4. FESEM pictures of Zn-La oxide nanoparticlesat different magnifications (2 µm and 1 µm).

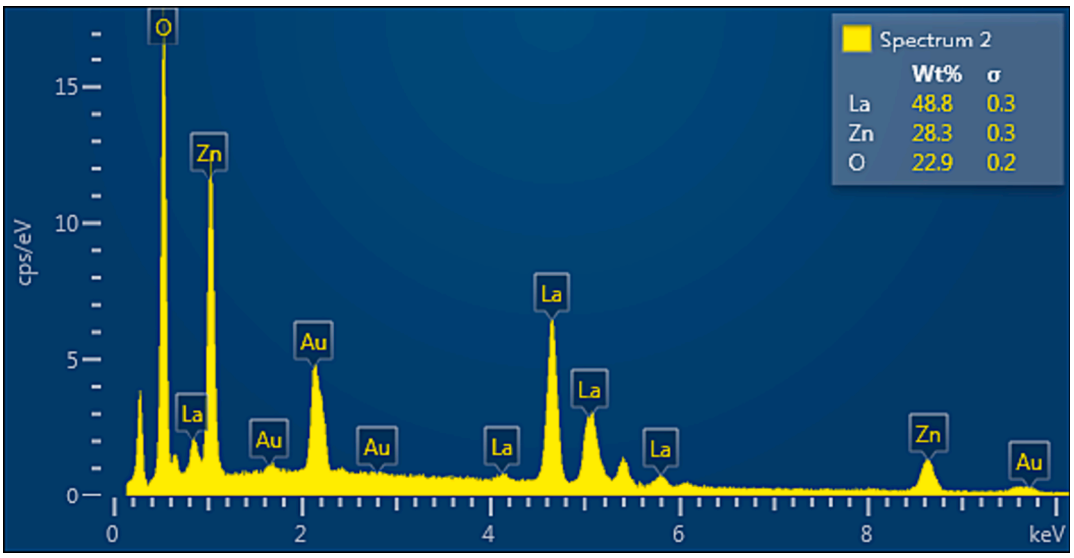

Fig. 5. EDX analysis of Zn-La oxide nanoparticles.

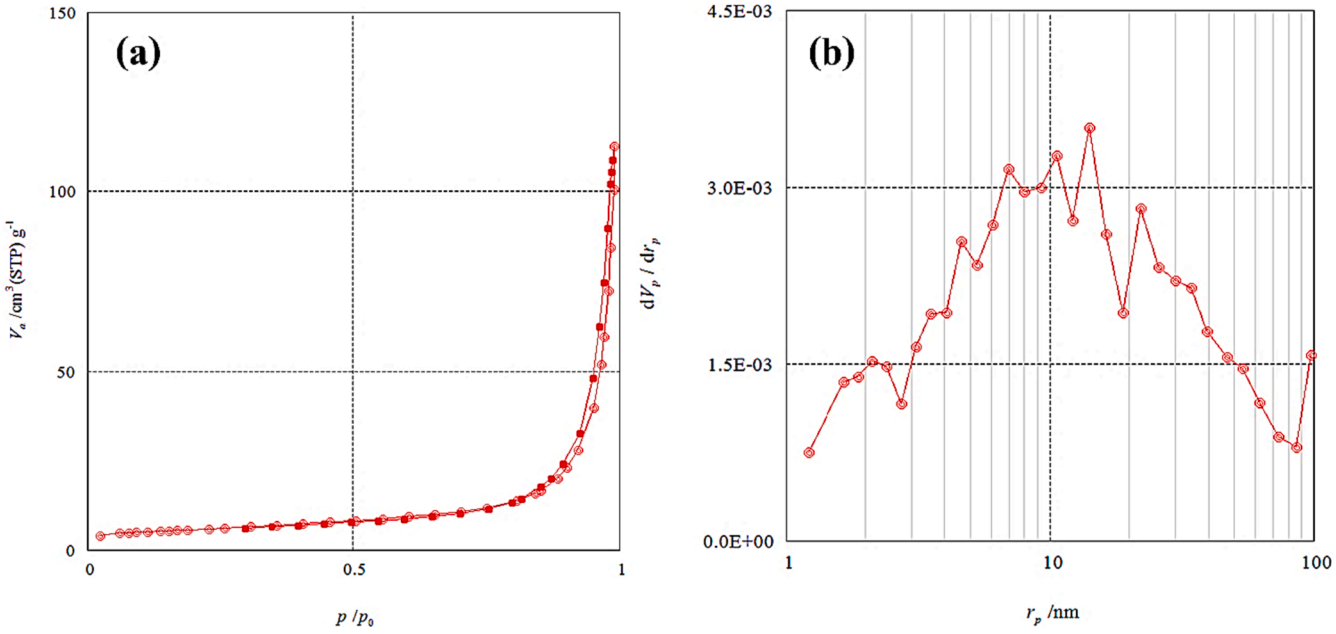

Fig. 6. (a) N_2 adsorption/desorption isotherm and (b) BJH pore size distribution of Zn-La oxides nanoparticles.

Table 3
Numerical values of BET analysis of Zn-La oxidesnanocatalyst.

BET plot		
V_m	4.6	cm^3(STP) g^{-1}
as,$_{BET}$	20.4	m^2 g^{-1}
C	1272.6	
Total pore volume (p/p_0 = 0.990)	0.17	cm^3 g^{-1}
Mean pore diameter	33.4	nm

active sites. These materials are typically prepared under mild reaction conditions, resulting in a lower production cost (Ramírez-Aparicio et al., 2021). The widespread use of amorphous catalysts in La-based systems for the photocatalysis processes is becoming increasingly prevalent (Liang et al., 2022).

3.2. Statistical analysis of the RSM approach

Diverse factors i.e. catalyst amount, solution pH, H_2O_2 dose, and UV power impact the MB dye degradation approach. Therefore, the influence of these factors was surveyed on MB dye degradation from aqueous suspension employing Zn-La oxide nanocatalyst. These characteristics were considered in three levels and the outcomes of the empirical procedure are given in Table 4. In this regard, 27 trials were generated, which is seen in this table. The outcomes of MB dye degradation efficiency for each test under various laboratory conditions along with the predicted quantities from the software are apparently noticed in Table 4. The highest MB dye degradation yield is observed to be 75.1%, achieved with a catalyst amount of 12 mg, solution pH of 9, H_2O_2 dose of 0.5, and UV power of 23. Moreover, the anticipated MB dye degradation yield through the RSM technique in these circumstances was 75.5%. Table 5 also illustrates the statistical outputs gained via the software. The p-value is a vital aspect depicting how a variable influences the process

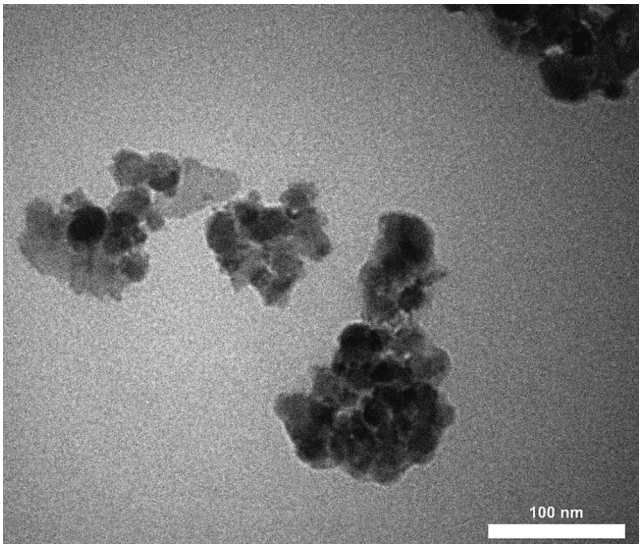

Fig. 7. TEM picture of Zn-La oxides nanoparticles.

Table 4
Design of experiment according to RSM-BBD approach.

Runs	Catalyst (mg)	pH	H_2O_2 (mL)	UV power (W)	MB degradation (%)
1	4	3	0.5	15	14.28
2	20	3	0.5	15	14.11
3	4	9	0.5	15	48.18
4	20	9	0.5	15	36.36
5	12	6	0.2	8	8.88
6	12	6	0.8	8	6.6
7	12	6	0.2	23	33.33
8	12	6	0.8	23	35.18
9	4	6	0.5	8	27.23
10	20	6	0.5	8	11.83
11	4	6	0.5	23	27.5
12	20	6	0.5	23	31.52
13	12	3	0.2	15	36.66
14	12	9	0.2	15	49.45
15	12	3	0.8	15	38.63
16	12	9	0.8	15	14.77
17	4	6	0.2	15	9.89
18	20	6	0.2	15	11.93
19	4	6	0.8	15	7.69
20	20	6	0.8	15	5.37
21	12	3	0.5	8	35.29
22	12	9	0.5	8	70.58
23	12	3	0.5	23	61.76
24	12	9	0.5	23	75.18
25	12	6	0.5	15	67.44
26	12	6	0.5	15	60.05
27	12	6	0.5	15	70.11

(Liang et al., 2022; Maleki et al., 2024a). Utilizing RSM, the p-values for key variables, namely catalyst amount, solution pH, H_2O_2 dosage, and UV power, influencing MB dye degradation with the Zn-La oxide nanocatalyst were determined. The p-values for the model and UV power factor were both less than 0.05, indicating their significance in MB dye degradation. Correspondingly, by comparing the interaction of these variables, it can be realized that the interaction of H_2O_2 dose and UV power has a p-value less than 0.05, illustrating that it has more effect on MB dye degradation, while the interaction of other factors i.e. catalyst amount and solution pH is not important on MB dye degradation yield as their p-values are more than 0.05 (Saraee et al., 2023). Besides, the same outcomes can be noticed through the F-value. The bigger the F-value for a factor, the more impact that variable has on MB dye degradation yield. Based on Table 5, the highest F-value was heeded for the

Table 5
ANOVA for data achieved from MB dye degradationyield by Zn-La oxides nanocatalyst.

Source	Sum of Squares	Df	Mean Square	F value	p-value Prob > F
Model	11618.43	12	968.20	9.26	0.0001
A-Catalyst amount	36.18	1	36.18	0.35	0.5657
B-pH	686.59	1	686.59	6.57	0.0226
C-H_2O_2	147.56	1	147.56	1.41	0.2546
D-UV	903.24	1	903.24	8.64	0.0108
AB	33.93	1	33.93	0.32	0.5779
AC	4.75	1	4.75	0.045	0.8342
AD	89.67	1	89.67	0.86	0.3701
BC	335.81	1	335.81	3.21	0.0947
BD	106.88	1	106.88	1.02	0.3291
A^2	6010.28	1	6010.28	57.49	< 0.0001
C^2	5429.69	1	5429.69	51.94	< 0.0001
D^2	584.03	1	584.03	5.59	0.0331
Residual	1463.67	14	104.55		
Lack of fit	1408.77	12	117.40	4.28	0.2050
Pure Error	54.90	2	27.45		
Cor total	13082.10	26			
R-Squared	0.8881		Std. Dev.	10.22	
Adj. R Squared	0.8022		C.V. %	30.36	
Adeq. Precision	9.893				

UV power variable (i.e., 8.6), displaying that this variable has the most remarkable impact on the MB dye degradation procedure. Furthermore, the R^2 values for MB dye degradation using Zn-La oxide nanocatalysts are all above 0.85, signifying the reliability of the results. Moreover, the p-value for MB dye degradation utilizing Zn-La oxide nanocatalysts is less than 0.05, the F-value is a substantial value (9.26) and the lack of fit is insignificant (4.28). These findings suggest that a 2nd-order polynomial relationship can be considered reliable for the studied system. In addition, this model has high accuracy as its C.V. amount is low (30.36). Hence, Eq. (3) demonstrates a vital model between the response (i.e., yield) and experimental variables (i.e., A, B, C, and D) for MB dye degradation utilizing Zn-La oxide nanocatalysts (Betiku and Adesina, 2013; Saraee et al., 2023). With this equation, the efficiency of MB dye degradation can be predicted under conditions beyond those examined in this study. Equation (3) can be utilized to calculate the expected MB dye degradation yield using the RSM technique in terms of the essential coded variables.

$$\begin{aligned} MBdegradation(\%) = &+65.87 - 1.74A + 7.59B - 3.51C + 8.86D \\ &- 2.91AB - 1.09AC + 4.73AD - 9.16BC \\ &- 5.16BD - 31.65A^2 - 30.08C^2 - 9.92D^2 \end{aligned} \quad (3)$$

Here, Y is the anticipated MB dye degradation yield and model variables denoted as A = catalyst amount, B = solution pH, C = H_2O_2dose and D = UV power.

Normal probability diagrams for MB dye degradation using Zn-La oxide nanocatalysts are presented in Fig. 8. The diagram shows a normal scatter between the predicted and empirical results, with points closely aligned along the line. This alignment suggests a strong indication that the model can be applied with a high level of significance (Maleki et al., 2024b; Betiku and Adesina, 2013).

3.3. The impact of photocatalytic factors on the degradation of MB dye

The influence of diverse variables and their interaction on MB dye degradation yield can be revealed in 3D diagrams. Fig. 9 exhibits the impact of effective parameters i.e. catalyst amount, solution pH, H_2O_2 dose, and UV power on MB dye degradation yield employing Zn-La oxide nanocatalysts. A crucial factor in MB dye degradation is catalyst amount, which has an enormous effect on MB dye degradation. Furthermore, this variable has an influential effect on the procedure

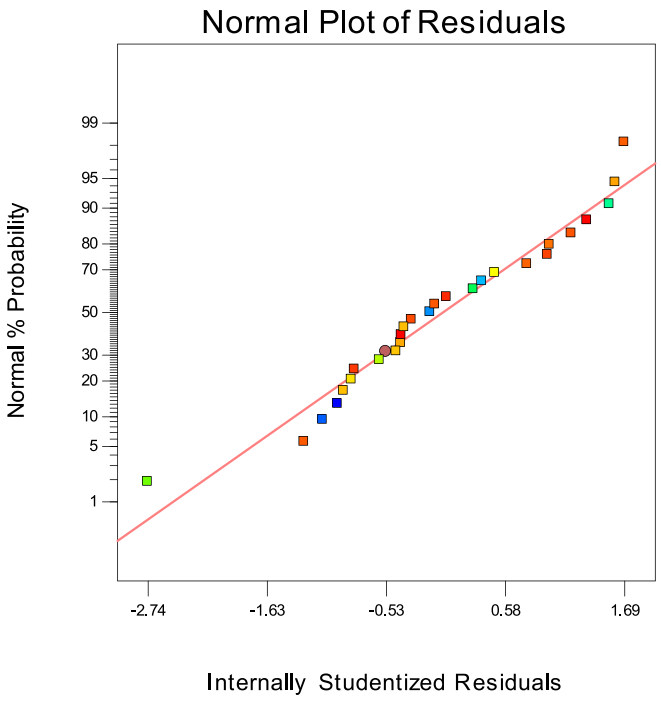

Fig. 8. Diagrams of normal probability from MB degradation using Zn-La oxides nanocatalyst.

economy, so its low amount can be more proper. Thus, the yield of MB dye degradation was ameliorated by increasing the catalyst amount from 4 to around 13 mg. The optimal dose, according to Fig. 9(a, b, c) was attained at 12 mg. At high catalyst amounts of Zn-La oxide nanocatalysts, the yield of MB dye degradation diminishes, likely due to catalyst particles obstructing the passage of UV light (Adesina et al., 2019). The high content of catalyst loading not only declines MB dye yield but also boosts the MB dye degradation expense (Almehizia et al., 2022). Nevertheless, the increment of catalyst amount has the opposite impact on the photocatalytic procedure because of the disruption in the MB dye degradation operation. As the catalyst amount is significantly increased, the turbidity of the mixture rises, leading to a reduction in the amount of UV light present. This decrease in UV light hampers the effective movement of particles on the surface of Zn-La oxide nanocatalysts, resulting in a decline in the overall process yield.

pH is another remarkable factor in MB dye degradation. Furthermore, experiments were conducted at various pH amounts (3 to 9); the outcomes are demonstrated in Fig. 9(a, d, e). According to the figures, the yield of MB dye degradation reduces from 3 to 9. As evident in the figure, the yield of MB dye degradation is enhanced by reducing the pH to acidic conditions. In acidic circumstances, the Zn-La oxide nanocatalysts' surface evolves positively charged because of the presence of H^+ ions in the mixture. Moreover, the surface of the pigment has a positive charge. Accordingly, an electrostatic bond is generated between the Zn-La oxide nanocatalysts and the MB, leading to an enhancement in the dye degradation yield (Zhou et al., 2022; Murshed et al., 2022).

Likewise, H_2O_2 boosts the generation acceleration of $OH^\bullet$ radicals and promotes the decomposition of combinations in low concentrations. This is attributed to the effective formation of $OH^\bullet$ and the inhibition of electron-hole pair recombination, as H_2O_2 acts as an electron acceptor. Besides, examining the impact of the H_2O_2 dose indicates that the MB dye degradation yield improves by decreasing the H_2O_2 dose from 0.8 to approximately 0.2. The optimal dose of H_2O_2 quantity was calculated at 0.52. The H_2O_2 dose is a critical parameter influencing the MB dye degradation yield, and a lower dose is preferable. As illustrated in Fig. 9 (b, d, f), the degradation yield of MB dye decreases with an increase in H_2O_2 dose. This could be attributed to recombination events facilitated by $OH^\bullet$ radicals and the inhibitory effect of higher H_2O_2 concentrations. Furthermore, the H_2O_2 can consume $OH^\bullet$ and form OOH ($H_2O_2 + OH^\bullet = OOH$), which has much less oxidation ability (Yu et al., 2021; Jahani et al., 2023).

Light intensity is considered one of the most important independent variables in the processes of MB photo-catalytic degradation. Fig. 9(c, e, f) reveals the effect of light intensity on the degradation of MB. These figures demonstrate that the percentage of MB dye degradation boosts with increasing UV power. It can be observed that the MB degradation percentage increased from 8 to 23 percent, then dropped to 61.5 percent again. the maximum value of efficiency of MB degradation was recorded (66%) at light power = 22 W. In photocatalysis, electrons within the particles of the photocatalyst require energy to move. This energy is derived from the incident radiation light. Consequently, there exists a direct relationship between the reaction speed constant and the intensity of light radiation. In other words, they are proportionally related as the light intensity increases, the excitation of electrons also increases. The generation of an ample quantity of active hydroxyl radicals increases as the number of excited electrons multiplies, leading to a higher rate of photocatalytic oxidation (Jahani et al., 2023; Chanu et al., 2019). It is noteworthy that photocatalytic rates may not necessarily increase with the rising light source power. This is because the photocatalytic degradation rate is influenced by various factors beyond light source power. The accumulation of non-desorbed matter on the photocatalyst surface can constrain the photocatalytic degradation rate, especially in the higher range of photocatalytic rates (Ibukun et al., 2019).

3.4. Optimization process

The design limitations were defined as follows: the four operational variables (A, B, C, & D) were constrained within specified ranges, and the objective for the MB degradation efficiency response (Zn-La oxide nanocatalyst) was set to maximize. From the 100 solutions generated by the software, the optimal solution was selected based on a desirability value of 1 and the highest MB degradation efficiency. Fig. 10 illustrates the optimal conditions for each operational factor. The maximum MB degradation was achieved under the reaction conditions of a catalyst amount of 12.05 mg, pH of 9, H_2O_2 dose of 0.44 mL for 45 min, and UV power of 23 W. Three tests were conducted under these optimal conditions, and the corresponding empirical MB degradation values using Zn-La oxide nanocatalyst were determined to be 72.3 ± 0.52%. It is evident that the actual values closely align with the software-anticipated values. Besides, following the identification of optimal reaction conditions, we conducted the photocatalytic removal of methylene blue using pure zinc oxide, attaining an efficiency of 61.7%. Comparative analysis between the results obtained with pure ZnO and the binary composite (Zn-La oxide) reveals that the addition of La has a positive impact on the methylene blue removal procedure.

3.5. Kinetic study of photocatalytic procedure by Zn-La oxide nanocatalysts

Reaction kinetics is a crucial property for assessing reaction rates and understanding the transformation mechanism of reactants into products. Kinetic models play a vital role in determining the reaction rate of a process. In this sense, Langmuir-Hinshelwood was employed to depict the kinetic study of the photocatalytic process of MB dye using Zn-La oxide nanocatalyst. The first-order kinetic equation proposed by the Langmuir-Hinshelwood model is represented by the following relationship (Eq. (4) (Alkaykh et al., 2020; Yan et al., 2022):

$$Ln\left(\frac{C_o}{C_t}\right) = k_1 t \tag{4}$$

By examining the slope of this plot, with zero as the intercept, the value of k_1 is determined (Ibukun et al., 2019). Notably, in 120 min, the

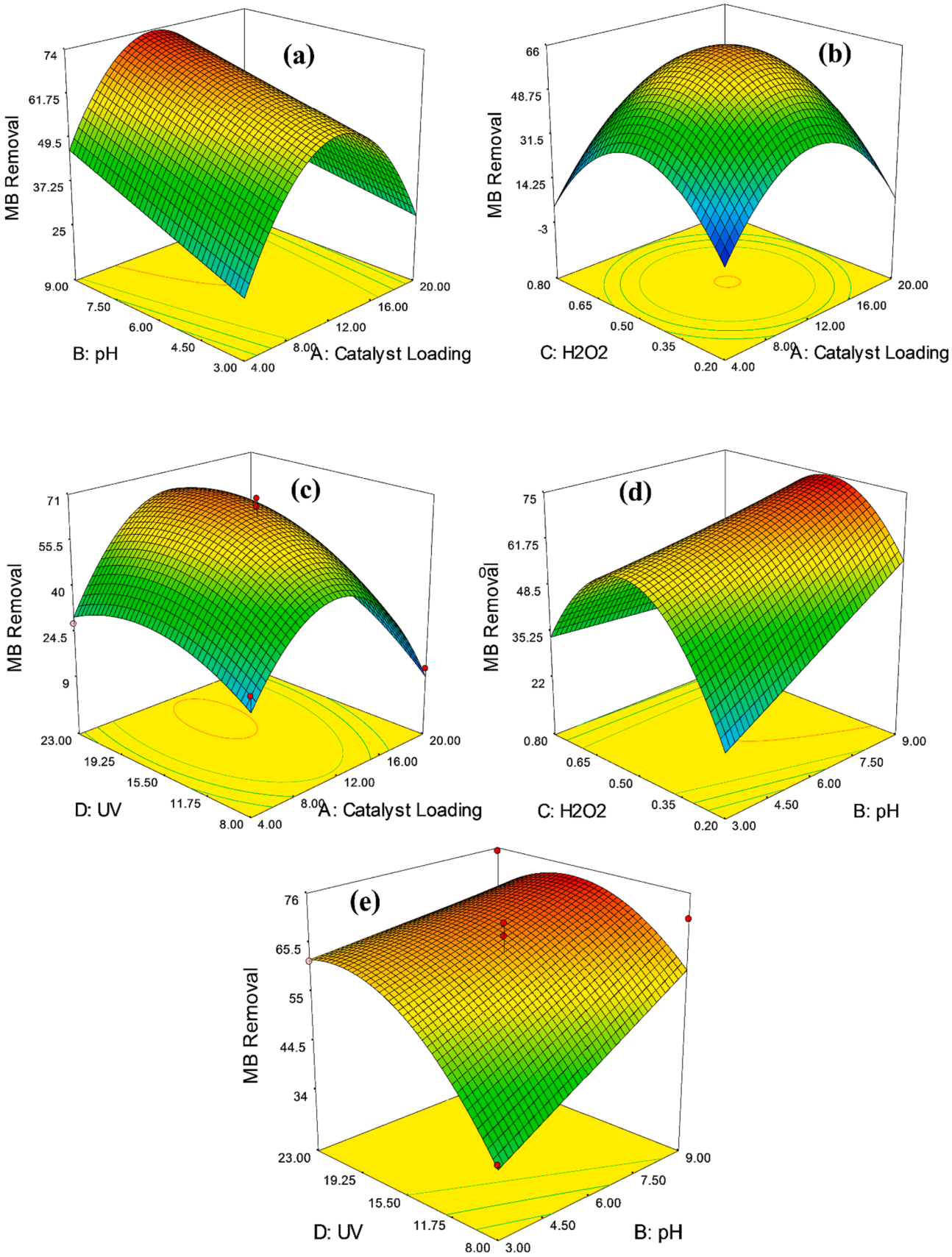

Fig. 9. 3D-diagrams of the impact of (a) catalyst amount-pH, (b) catalyst amount-H_2O_2dose, (c) catalyst amount-UV power (d) H_2O_2 dose- pH, (e) pH-UV power on MB dye degradationyield utilizing Zn-La oxide nanocatalysts.

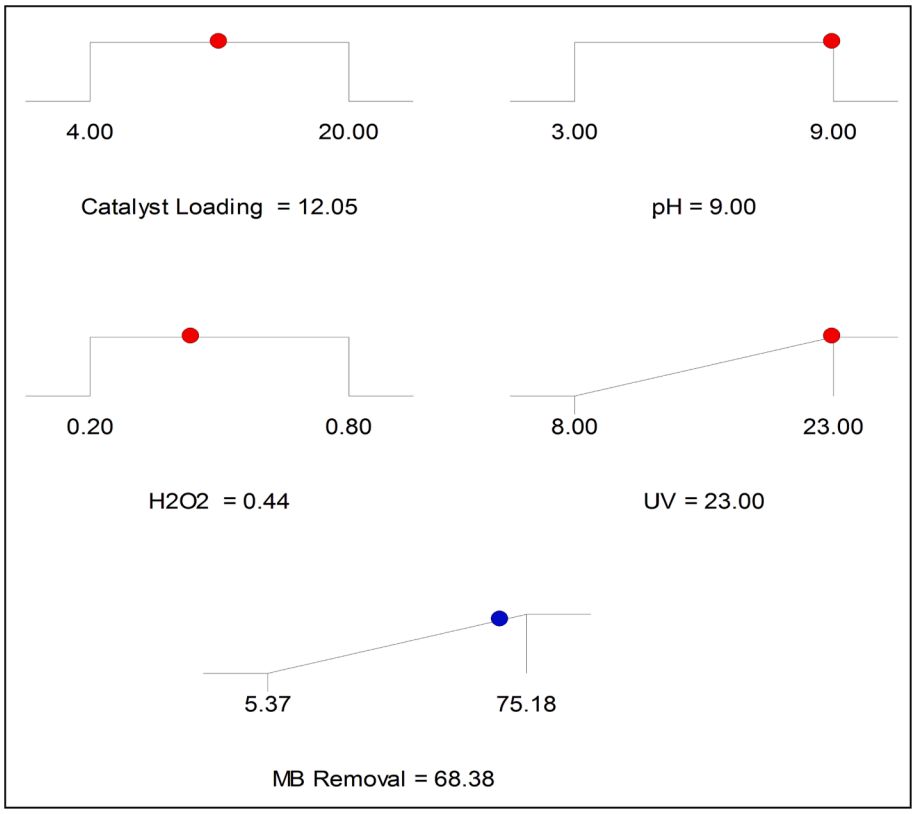

Fig. 10. RSM-BBD predicted optimal process point and their respective MB removal.

removal efficiency of methylene blue reached 98.8%, as shown in Fig. 11 (b). The photo-degradation kinetics of methylene blue dye by Zn-La oxide nanocatalyst was determined by plotting Ln C_o/C vs. irradiation time. According to Fig. 11(a), the rate constant (k) for the photocatalytic degradation of methylene blue is 0.0363 min^{-1}, and the correlation coefficient (R^2) is 0.9917. Furthermore, the R^2 values at all dye concentrations indicate that the model accurately fits the photocatalytic data, as their values are close to one.

3.6. Stability of Zn-La oxide nanocatalyst

The stability of nanocatalysts plays a crucial role in their application on large scales (Maleki et al., 2024a; Maleki and Esmaeili, 2023a). The stability investigation for the Zn-La oxide nanocatalysts was conducted in five rounds, and the outcomes are indicated in Fig. 12. The studies were executed at under optimal points, i.e. catalyst amount of 12.05 mg, pH of 9, H_2O_2 dose of 0.44 mL, UV power of 23 W, and time of 120 min. As displayed, the degradation percent of MB dye yield declined by 93.48% (only a 5.40% decrease), demonstrating that the stability has reduced by a negligible amount. Consequently, the Zn-La oxide nanocatalysts have considerable recyclability and can be utilized in numerous runs. Saraee et al. (2023) surveyed the degradation of MB employing biochar/Ag nanocatalysts in various contents of biochar and Ag (1:2 and 1:3). After five rounds, the removal amount of MB utilizing biochar/Ag nanocatalysts lowered from 94.7 to 88% (6.7% decline), indicating the stability of this nanocatalyst compared to this work. Also, Jahani et al. (2023) explored the degradation of reactive red 19 utilizing milkvetch-derived biochar via ZnO–Ce nanoparticle under UV light. Remarkably, after five cycles, the degradation efficiency of reactive red 19 only decreased by 6.08%.

3.7. Comparison of the current study with other research

An examination of the study background reveals a scarcity of research on the degradation of MB dye using UV light. To the best of our knowledge, the simultaneous application of Zn-La oxide nanocomposites and UV irradiation for MB dye degradation is reported for the first time in this scientific study. Generally, UV irradiation is considered more suitable than sunlight. Additionally, Zn-La oxide nanocomposites exhibit promising photocatalytic performance for MB degradation in wastewater. As indicated in Table 6, the present research has demonstrated significant efficiency in the rapid degradation of MB dye compared to other photocatalysts.

3.8. Photocatalytic mechanism

The photocatalytic activity of the Zn-La oxide nanocomposites for MB decolorization was primarily due to electron hole pair recombination inhibition by charge transfer processes. Fig. 13 showed the proposed energy band structure diagram of the Zn-La oxide photocatalysts. When the Zn-La oxide nanocomposites was formed, the electron transfer occurred from ZnO to lanthanum oxide while the holes transfer occurred from La^{+2}/La^{+3} oxide to ZnO until the system obtained equalization. When the Zn-La oxide photocatalysts were irradiated by UV light with photon energy higher than or equal to the band gaps of ZnO and lanthanum oxide, the electrons (e) in the valence band (VB) could be excited to the conduction band (CB) with simultaneous generation of the same amount of holes (h^+) in the VB (Eq. (5). Shelar et al. reported that the photo-generated holes and $^{\cdot}OH^*$ are the major species of Ag doped ZnO while, the O_2^{*-} radical acts as supportive species in the degradation of MB (Shelar et al., 2020; Alkaykh et al., 2020). The oxidants such as H_2O_2 have been suggested to promote the efficiency of MB dye degradation (Eq. (6). H_2O_2 can employ the excited electrons (Eq. (7) and therefore hinder the charge recombination (Kraidi et al., 2023). These results lead to the conclusion that hydroxyl radicals and holes play a crucial role in the photodegradation of MB dye.

$$Photocatalyst + hv \rightarrow e^- + h^+ \quad (5)$$

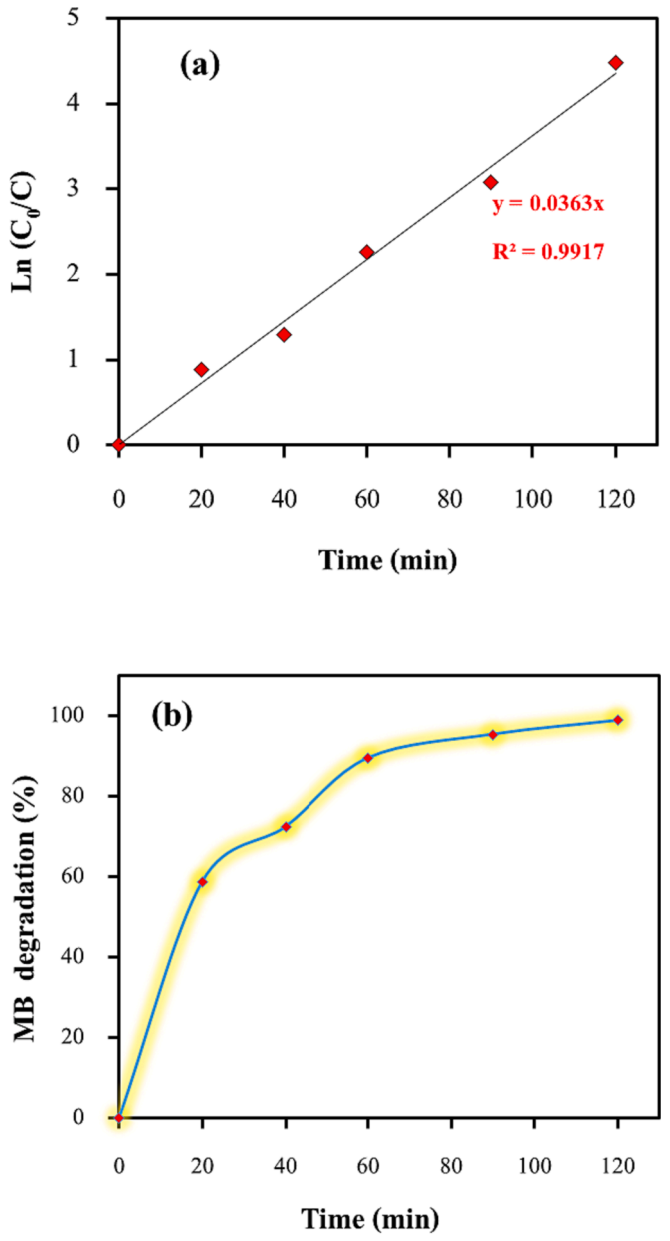

Fig. 11. (a) Kinetic outcomes (b) degradation of MB dye -time via Zn-La oxide nanocatalyst.

$$H_2O_2 + hv \rightarrow 2OH^* \quad (6)$$

$$H_2O_2 + e^- \rightarrow OH^- + OH^* \quad (7)$$

$$e^- + O_2 \rightarrow O_2^{*-} \quad (8)$$

$$h^+ + OH^- \rightarrow OH^* \quad (9)$$

$$h^+ + Pollutant \rightarrow Degradation products \quad (10)$$

$$OH^* + Pollutant \rightarrow Degradation products \quad (11)$$

Based on these findings, the following mechanism for MB dye degradation is proposed. Equation (5) shows the formation of electrons and holes upon UV irradiation on the Zn-La oxide nanocatalyst surface. Equations (8) and (9) illustrate the formation of superoxide (O^{2*}) and hydroxyl (OH*) radicals, respectively. Equations (10) and (11) reveal the degradation of MB dye by holes and hydroxyl radicals, respectively.

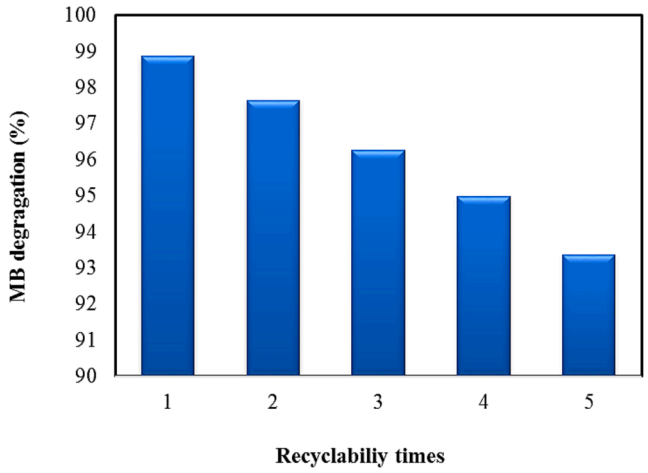

Fig. 12. Stability of Zn-La oxide nanocatalysts in the removal of MB.

Table 6
Comparison of the photocatalytic performance of diverse nanoparticles in the degradation of MB dye.

Photocatalyst	Reaction time (min)	Efficiency (%)	Light source	Power lamp (W)	Ref.
ZnO/ MWCNTs	25	91.86	UV	–	(Abbasi et al., 2019)
ZSM-5 zeolite@ ZnO	120	94.09	LED	50	(Nazari et al., 2023)
ZnO–SnO_2 (ZS)	60	91.5	UV	–	(Lin et al., 2018)
ZnO	70	100	UV	–	(Almehizia et al., 2022)
ZnO/Ti_2C	130	99.16	UV	100	(Zhou et al., 2022)
ZnO/biochar	20	95.19	UV	–	(Yu et al., 2021)
Mn-doped ZnO	120	99	UV	100	(Chanu et al., 2019)
TiO_2-MoS_2	80	86.42	UV	–	(Ibukun et al., 2019)
$MnTiO_3$	240	75	Sun light	–	(Alkaykh et al., 2020)
ZnO@GO	150	97.56	UV		(Elshahawy et al., 2023)
Fe_3O_4/ZnO	100	88.5	UV		(Elshypany et al., 2021)
ZnO/rGO	180	98.05	UV		(Kumar et al., 2021)
NiO @GLY	100	99	UV		(Shelar et al., 2020)
Zn-La oxide	120	98.8	UV		This study

Moreover, biocompatibility of pure ZnO, lanthanum oxide and Zn-La oxide catalyst has been done in past studies. Their results showed that the Zn-La oxide nanocatalyst potential antibacterial activity was higher than that of ZnOnanoparticles alone, and increasing the concentration of Zn-La oxide nanocatalyst also increased the antibacterial activity (Senthilkumar et al., 2023; Barman, 2015). Brabu, et al. (2015) scrutinized the antibacterial activity of ZnO and Zn-La oxide nanoparticles. The study evaluated the antibacterial activity of ZnO and Zn-La oxide nanocatalysts against both gram-positive bacteria (*S. aureus* and *B. subtilis*) and gram-negative bacteria (*E. coli* and *K. pneumonia*) strains. Besides, the Zn-La oxide nanocatalyst illustrated higher antibacterial activity compared to ZnO nanoparticles alone, and a boost in the concentration of Zn-La oxide nanocatalyst correlated with enhanced antibacterial performance. Additionally, both ZnO and Zn-La oxide nanocatalysts demonstrated potential in treating human breast cancer

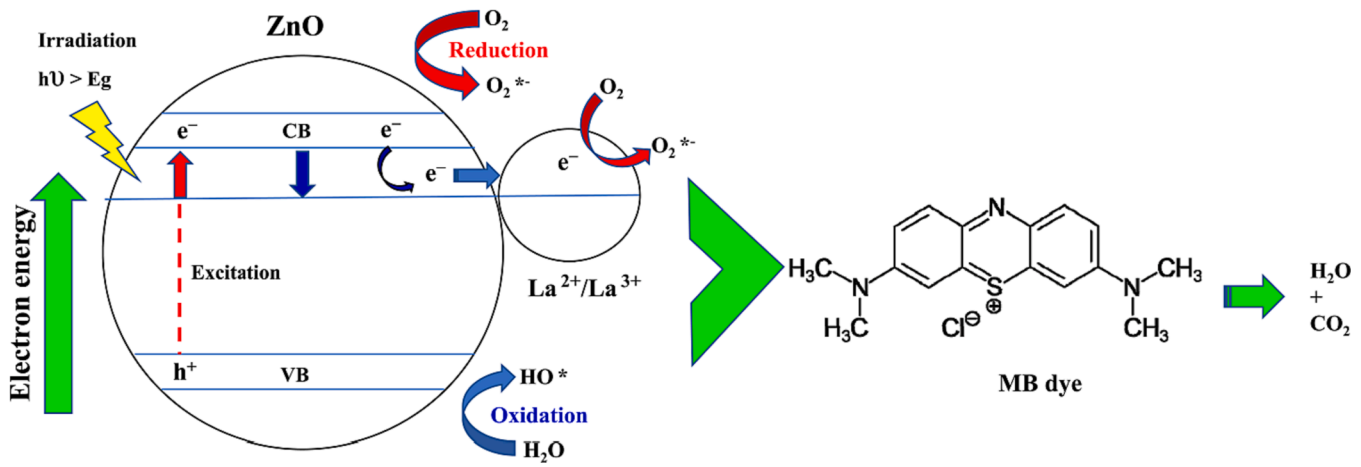

Fig. 13. Mechanism of photocatalytic degradation of MB dye using Zn-La oxide nanocatalyst.

cell lines, with the Zn-La oxide nanocatalyst displaying greater anticancer activity at lower concentrations. These findings suggest that Zn-La oxide nanocatalyst could serve as promising agents for antibacterial and anticancer utilization, making them appropriate for usage in biomedical contexts.

4. Conclusion

In this study, the performance of Zn-La oxide nanocatalysts was examined for the UV irradiation-induced degradation of MB dye. Surface characteristics of the Zn-La oxide nanocatalysts were analyzed using FESEM, FTIR, XRD, BET-BJH, EDX, and TEM techniques. The BET-BJH analysis revealed a specific surface area of 20.43 m^2/g for the Zn-La oxide nanocatalyst. Employing a catalyst amount of 12.05 mg, pH of 9, H_2O_2 dose of 0.44 mL, and UV power of 23 W for 45 min using the RSM procedure, the highest degradation yield of MB dye (75.56%) was achieved. Furthermore, under these conditions, the MB degradation yield reached 98.8% after 120 min. Kinetic analysis indicated that the pseudo-first-order kinetic model was fitting for MB dye degradation. The introduction of H_2O_2 resulted in enhanced removal and reduced recombination of the generated electron-hole pairs. Moreover, the recyclability assessment of the Zn-La oxide nanocatalyst revealed only a 5.4% decline in stability after five cycles. This study highlights the potential application of Zn-La oxide nanocatalysts as effective photocatalysts for improved MB dye degradation in suspension mixtures.

Availability of data and materials

The datasets used and/or analysed during the current study are available from the corresponding author on reasonable request.

Ethical approval

Not applicable.

Authors contributions

All authors contributed to the study conception and design. Material preparation, data collection and analysis were performed by **BasirMaleki**, **Majeed Khudhair Jasim**, **Mohsen Mansouri**, and **Tahseen Hameed Khlaif**. The first draft of the manuscript was written by **BasirMaleki**and all authors commented on previous versions of the manuscript. All authors read and approved the final manuscript. All authors are fully aware of this manuscript and have permission to submit the manuscript for possible publication.

Funding

M. M. thanks the University of Ilam, for the award research fellowship.

References

Abbasi, S., 2023. Magnetic photocatalysts based on graphene oxide: synthesis, characterization, application in advanced oxidation processes and response surface analysis. Appl. Water Sci. 13, 128. https://doi.org/10.1007/s13201-023-01931-4.

Abbasi, S., Ekrami-Kakhki, M.S., Tahari, M.M., 2019. The influence of ZnO nanoparticles amount on the optimisation of photo degradation of methyl orange using decorated MWCNTs. Prog. Ind. Ecol. 13, 3–15. https://doi.org/10.1504/PIE.2019.098760.

Abbasi, S., Ahmadpoor, A., Imani, M., Ekrami-Kakhki, M.S., 2020. Synthesis of magnetic Fe_3O_4@ZnO@graphene oxide nanocomposite for photodegradation of organic dye pollutant. Int. J. Environ. Anal. Chem. 100, 225–240. https://doi.org/10.1080/03067319.2019.1636038.

Adesina, O.A., Abdulkareem, F., Yusuff, A.S., Lala, M., Okewale, A., 2019. Response surface methodology approach to optimization of process parameter for coagulation process of surface water using Moringa oleifera seed. S. Afr. J. Chem. Eng. 28, 46–51. https://doi.org/10.1016/j.sajce.2019.02.002.

Afmataj, D., Kordera, O., Maragkaki, A., Tzanakakis, V.A., Pashalidis, I., Kalderis, D., Anastopoulos, I., 2023. Adsorption of reactive Red 120 dye by polyamide nylon 6 microplastics: isotherm, kinetic, and thermodynamic analysis. Water 15 (6), 1137. https://doi.org/10.3390/w15061137.

Alkaykh, S., Mbarek, A., Ali-Shattle, E.E., 2020. Photocatalytic degradation of methylene blue dye in aqueous solution by $MnTiO_3$ nanoparticles under sunlight irradiation. Heliyon 6 (4), 03663. https://doi.org/10.1016/j.heliyon.2020.e03663.

Almehizia, A.A., Al-Omar, M., Naglah, A., Bhat, M.A., Al-Shakliah, N.S., 2022. Facile synthesis and characterization of ZnO nanoparticles for studying their biological activities and photocatalytic degradation properties toward methylene blue dye. Alex. Eng. J. 61, 2386–2395. https://doi.org/10.1016/j.aej.2021.06.102.

Anandan, S., Vinu, A., Sheeja, K.L.P., Gokulakrishnan, N., Srinivasu, P., Mori, T., Murugesan, V., Sivamurugan, V., Ariga, K., 2007. Photocatalytic activity of La-doped ZnO for the degradation of monocrotophos in aqueous suspension. J. Mol. Catal. A Chem. 266, 149–157. https://doi.org/10.1016/j.molcata.2006.11.008.

Ashrafi, S.D., Safari, G.H., Sharafi, K., Kamani, H., Jaafari, J., 2021. Adsorption of 4-Nitrophenol on calcium alginate-multiwall carbon nanotube beads: modeling, kinetics, equilibriums and reusability studies. Int. J. Biol. Macromol. 185, 66–76. https://doi.org/10.1016/j.ijbiomac.2021.06.081.

Barman, A., 2015. Review on biocompatibility of ZnO nano particles. In: Gupta, S., Bag, S., Ganguly, K., Sarkar, I., Biswas, P. (Eds.) Advancements of Medical Electronics. Lecture Notes in Bioengineering. Advancements of Medical Electronics, pp. 343-352. doi: 10.1007/978-81-322-2256-9_32.

Betiku, E., Adesina, O.A., 2013. Statistical approach to the optimization of citric acid production using filamentous fungus Aspergillus niger grown on sweet potato starch hydrolysate. Biomass Bioenergy 55, 350–354. https://doi.org/10.1016/j.biombioe.2013.02.034.

Brabu, B., Haribabu, S., Revathy, M., Anitha, S., Thangapandiyan, M., Navaneethakrishnan, K.R., Gopalakrishnan, C., Murugan, S.S., Kumaravel, T.S., 2015. Biocompatibility studies on lanthanum oxide nanoparticles. Toxicol. Res. 4 https://doi.org/10.1039/c4tx00198b.

Chaker, H., Ameur, N., Saidi-Bendahou, K., Djennas, M., Fourmentin, S., 2021. Modeling and Box-Behnken design optimization of photocatalytic parameters for efficient removal of dye by lanthanum-doped mesoporous TiO_2. J. Environ. Chem. Eng. 9, 2213–3437. https://doi.org/10.1016/j.jece.2020.104584.

Chanu, L.A., Singh, W.J., Singh, K.J., Devi, K.N., 2019. Effect of operational parameters on the photocatalytic degradation of Methylene blue dye solution using manganese

doped ZnO nanoparticles. Results Phys. 12, 1230–1237. https://doi.org/10.1016/j.rinp.2018.12.089.
Chen, Y., Yuan, T., Wang, F., Hu, J., Tu, W., 2016. Magnetically separable Fe_3O_4@ TiO_2 nanospheres: preparation and photocatalytic activity. J. Mater. Sci. Mater. Electron. 27, 9983–9988. https://doi.org/10.1007/s10854-016-5330-7.
Elfeky, A.S., Youssef, H.F., Elzaref, A.S., 2020. Adsorption of dye from wastewater onto ZnO nanoparticles-loaded zeolite: kinetic, thermodynamic and isotherm studies. Z. fur Phys. Chem. 234 (2), 255–278. https://doi.org/10.1515/zpch-2018-1342.
Elshahawy, M.F., Ahmed, N.A., Mohamed, R.D., El-Hag Ali, A., Raafat, A.I., 2023. Radiation synthesis and photocatalytic performance of floated graphene oxide decorated ZnO/alginate-based beads for methylene blue degradation under visible light irradiation. Int. J. Biol. Macromol. 243, 125121 https://doi.org/10.1016/j.ijbiomac.2023.125121.
Elshypany, R., Selim, H., Zakaria, K., Moustafa, A.H., Sadeek, S.A., Sharaa, S.I., Raynaud, P., Nada, A.A., 2021. Elaboration of Fe_3O_4/ZnO nanocomposite with highly performance photocatalytic activity for degradation methylene blue under visible light irradiation. Environ. Technol. Innov. 23, 101710 https://doi.org/10.1016/j.eti.2021.101710.
Etemadi, F., Afzali, D., Fathirad, F., 2021. Design of acrylic acid/nanoclay grafted polysaccharide hydrogels as superabsorbent for controlled release of chlorpyrifos. Appl. Clay Sci. 211, 106194 https://doi.org/10.1016/j.clay.2021.106194.
Fathirad, F., Ziaadini, F., Mostafavi, A., Shamspur, T., 2021. Three-layer magnetic nanocomposite containing semiconductor nanoparticles as catalyst for dye removal from water solutions under visible light. Iran. J. Chem. Chem. Eng. 40, 1749–1756. https://doi.org/10.30492/IJCCE.2020.122646.4012.
Hajiali, M., Farhadian, M., Aflaki, S., Davari, N., 2021. Application of TiO_2/$ZnFe_2O_4$/glycine nanocatalyst to the treatment of methyl orange dye from aqueous solution: impacts of dissolved mineral salts on dye removal efficiency. Sci. Iran. 28 (3), 1464–1477. https://doi.org/10.24200/SCI.2021.56415.4715.
Hossein Panahi, A., Meshkinian, A., Ashrafi, S.D., Khan, M., Naghizadeh, A., Abi, G., Kamani, H., 2020. Survey of sono-activated persulfate process for treatment of real dairy wastewater. Int. J. Environ. Sci. Technol. 17, 93–98. https://doi.org/10.1007/s13762-019-02324-4.
Ibukun, O., Evans, P.E., Dowben, P.A., Jeong, H.K., 2019. Titanium dioxide-molybdenum disulfide for photocatalytic degradation of methylene blue. Chem. Phys. 525, 110419 https://doi.org/10.1016/j.chemphys.2019.110419.
Jahani, F., Maleki, B., Mansouri, M., Noorimotlagh, Z., Mirzaee, S.A., 2023. Enhanced photocatalytic performance of milkvetch-derived biochar via ZnO–Ce nanoparticle decoration for reactive blue 19 dye removal. Sci. Rep. 13, 17824. https://doi.org/10.1038/s41598-023-45145-9.
Jian, S., Tian, Z., Hu, J., Zhang, K., Zhang, L., Duan, G., Yang, W., Jiang, S., 2022. Enhanced visible light photocatalytic efficiency of La-doped ZnO nanofibers via electrospinning-calcination technology. Adv. Powder Mater 1, 100004. https://doi.org/10.1016/j.apmate.2021.09.004.
Khan, I., Saeed, K., Zekker, I., Zhang, B., Hendi, A.H., Ahmad, A., 2022. Review on methylene blue: its properties, uses, toxicity and photodegradation. Water 14 (2), 242. https://doi.org/10.3390/w14020242.
Kraidi, A.A., Mansouri, M., Karamian, E., 2023. The synergetic effect of lanthanide (La and Ce) and N co-doping of ZnO NPs for high-rate photocatalytic phenol degradation. Environ. Sci. Pollut. Res. 30 (9), 24168–24178. https://doi.org/10.1007/s11356-022-23729-8.
Kumar, S., Kaushik, R.D., Purohit, L.P., 2021. Novel ZnO tetrapod-reduced graphene oxide nanocomposites for enhanced photocatalytic degradation of phenolic compounds and MB dye. J. Mol. Liq. 327, 114814 https://doi.org/10.1016/j.molliq.2020.114814.
Law, L., Lim, Z.X.S., Chan, Y.Y., Shuit, S.H., Chong, W.C., Lai, C.W., 2021. Enhanced photocatalytic degradation of methyl orange by coconut shell–derived biochar composites under visible LED light irradiation. Environ. Sci. Pollut. Res. 28 (21), 27457–27473. https://doi.org/10.1007/s11356-020-12251-4.
Liang, H., Esmaeili, H., 2021. Application of nanomaterials for demulsification of oily wastewater: a review study. Environ. Technol. Innov. 22, 101498 https://doi.org/10.1016/j.eti.2021.101498.
Liang, H., Li, J., Shen, X., Cao, B., Zhu, J., Geng, B., Zhu, S., Li, W., 2022. The study of amorphous La@Mg catalyst for high efficiency hydrogen storage. Int. J. Hydrogen Energy 47, 18404–18411. https://doi.org/10.1016/j.ijhydene.2022.04.032.
Lin, J., Luo, Z., Lio, J., Li, P., 2018. Photocatalytic degradation of methylene blue in aqueous solution by using ZnO-SnO_2 nanocomposites. Mater. Sci. Semicond. Process. 87, 24–31. https://doi.org/10.1016/j.mssp.2018.07.003.
Maleki, B., Ashraf Talesh, S.S., 2021. Pour point and yield simultaneous improvement of alkyl esters produced by ultrasound-assisted in the presence of αFe_2O_3/ZnO: RSM approach. Fuel 298, 120827. https://doi.org/10.1016/j.fuel.2021.120827.
Maleki, B., Esmaeili, H., 2023a. Ultrasound-assisted conversion of waste frying oil into biodiesel using Al-doped ZnOnanocatalyst: Box-Behnken design-based optimization. Renew. Energy 209, 10–26. https://doi.org/10.1016/j.renene.2023.03.119.
Maleki, B., Ashraf Talesh, S.S., Mansouri, M., 2022. Comparison of catalysts types performance in the generation of sustainable biodiesel via transesterification of various oil sources: a review study. Materials Today Sustain. 18, 100157 https://doi.org/10.1016/j.mtsust.2022.100157.
Maleki, B., Yatish, K.V., Ashraf Talesh, S.S., Esmaeili, H., Mohan, S., Balakrishna, G.R., 2023a. A novel biomass derived activated carbon mediated AC@ ZnO/NiO bifunctional nanocatalyst to produce high-quality biodiesel from dairy industry waste oil: CI engine performance and emission. Chem. Eng. J. 467, 143399 https://doi.org/10.1016/j.cej.2023.143399.
Maleki, B., Esmaeili, H., Mansouri, M., Kumar, D., Singh, B., 2023b. Enhanced conversion of dairy waste oil to biodiesel via novel and highly reactive UiO-66-NH_2/ZnO/TiO_2 nano-catalyst: optimization, kinetic, thermodynamic and diesel engine studies. Fuel 340, 126901. https://doi.org/10.1016/j.fuel.2022.126901.
Maleki, B., Esmaeili, H., 2023b. Application of Fe_3O_4/SiO_2@ZnO magnetic composites as a recyclable heterogeneous nanocatalyst for biodiesel production from waste cooking oil: response surface methodology. Ceram. Int. 49, 11452–11463. https://doi.org/10.1016/j.ceramint.2022.11.344.
Maleki, B., Yatish, K.V., Esmaeili, H., Haddadi, M., Prakash, R.M., Balakrishna, G.R., 2024a. Novel Co_3O_4 decorated with rGO nanocatalyst to boost microwave-assisted biodiesel production and as nano-additive to enhance the performance-emission characteristics of diesel engine. Energy 289, 129944. https://doi.org/10.1016/j.energy.2023.129944.
Maleki, B., Yatish, K.V., Muthusamy, B., Esmaeili, H., 2024b. A cleaner approach towards magnetically assisted-electrolysis of biodiesel production using novel $MnFe_2O_4$@ sawdust derived biochar nanocatalyst and its performance on a CI engine. Energ. Conver. Manage. 299, 117829 https://doi.org/10.1016/j.enconman.2023.117829.
Mangeli, A., Mostafavi, A., Shamspur, T., 2021. Decontamination of fenitrothion from aqueous solutions using rGO/MoS_2/Fe_3O_4 magnetic nanosorbent: synthesis, characterization and removal application. J. Environ. Health Sci. Eng. 19, 1505–1511. https://doi.org/10.1007/s40201-021-00706-w.
Mazierski, P., Lisowski, W., Grzyb, T., Winiarski, M.J., Klimczuk, T., Mikołajczyk, A., Flisikowski, J., Hirsch, A., Kołakowska, A., Puzyn, T., 2017. Enhanced photocatalytic properties of lanthanide-TiO_2 nanotubes: an experimental and theoretical study. Appl. Catal. B Environ. 205, 376–385. https://doi.org/10.1016/j.apcatb.2016.12.044.
Mohamed, F., Hassaballa, S., Shaban, M., Ahmed, A.M., 2022. Highly efficient photocatalyst fabricated from the chemical recycling of iron waste and natural zeolite for super dye degradation. Nanomaterials 12 (2), 235. https://doi.org/10.3390/nano12020235.
Murshed, M.K., Dursun, A.Y., Dursun, G., 2022. Application of response surface methodology on photocatalytic degradation of Astrazon Orange G dye by ZnO photocatalyst: internal mass transfer effects. Chem. Eng. Res. Des. 188, 27–38. https://doi.org/10.1016/j.cherd.2022.09.038.
Nazari, S., Zare Aliabadi, H., Mansouri, M., Maleki, B., Bayati, B., 2023. The removal of methylene blue from aqueous solution using prepared ZSM-5 zeolite@ZnO nanoflowers under LED irradiation. Iran. J. Chem. Chem. Eng. 42 https://doi.org/10.30492/IJCCE.2023.2003412.6052.
Noorimotlagh, Z., Kazeminezhad, I., Jaafarzadeh, N., Ahmadi, M., Ramezani, Z., 2020. Improved performance of immobilized TiO_2 under visible light for the commercial surfactant degradation: role of carbon doped TiO_2 and anatase/rutile ratio. Catal. Today 348, 277–289. https://doi.org/10.1016/j.cattod.2019.08.051.
Norabadi, E., Hossein Panahi, A., Ghanbari, R., Meshkinian, A., Kamani, H., Ashrafi, S.D., 2020. Optimizing the parameters of awmoxicillin removal in a photocatalysis/ozonation process using Box-Behnken response surface methodology. Desalin. Water Treat. 192, 234–240. https://doi.org/10.5004/dwt.2020.25728.
Phuruangrat, A., Wannapop, S., Sakhon, T., Kuntalue, B., Thongtem, T., Thongtem, S., 2023. Characterization and photocatalytic properties of $BiVO_4$ synthesized by combustion method. J. Mol. Struct. 1274, 134420 https://doi.org/10.1016/j.molstruc.2022.134420.
Pinchujit, S., Phuruangrat, A., Wannapop, S., Sakhon, T., Kuntalue, B., Thongtem, T., Thongtem, S., 2022. Synthesis and characterization of heterostructure Pt/Bi_2WO_6 nanocomposites with enhanced photodegradation efficiency induced by visible radiation. Solid State Sci. 134, 107064 https://doi.org/10.1016/j.solidstatesciences.2022.107064.
Ramírez-Aparicio, J., Samaniego-Benítez, J.E., Murillo-Tovar, M.A., Benítez-Benítez, J. L., Muñoz-Sandoval, E., García-Betancourt, M.L., 2021. Removal and surface photocatalytic degradation of methylene blue on carbon nanostructures. Diam. Relat. Mater. 119, 108544 https://doi.org/10.1016/j.diamond.2021.108544.
Ruzimuradov, O., Hojamberdiev, M., Fasel, C., Riedel, R., 2017. Fabrication of lanthanum and nitrogen-Co-doped $SrTiO_3$-TiO_2 heterostructuredmacroporous monolithic materials for photocatalytic degradation of organic dyes under visible light. J. Alloy. Compd. 699, 144–150. https://doi.org/10.1016/j.jallcom.2016.12.355.
Saraee, H., Mansouri, M., Maleki, B., Esmaeili, H., 2023. Modified nanoarchitectonics of activated carbon derived from the *Astragalus* shrub for efficient photocatalytic degradation of methylene blue from water. Int. J. Environ. Anal. Chem. https://doi.org/10.1080/03067319.2023.2220288.
Senthilkumar, G., Sakthivelu, A., Abdur Rahman, M., Parameswar, P., 2023. Enhancement of antibacterial and anticancer properties lanthanum insight into zinc oxide nanoparticles prepared via coprecipitation process. Inorg. Chem. Commun. 155, 111081 https://doi.org/10.1016/j.inoche.2023.111081.
Shelar, S.G., Mahajan, V.K., Patil, S.P., 2020. Effect of doping parameters on photocatalytic degradation of methylene blue using Ag doped ZnO nanocatalyst. SN Appl. Sci. 2, 820. https://doi.org/10.1007/s42452-020-2634-2.
Shwetharani, R., Sakar, M., Chandan, H.R., Balakrishna, R.G., 2018. Observation of simultaneous photocatalytic degradation and hydrogen evolution on the lanthanum modified TiO_2 nanostructures. Mater. Lett. 218, 262–265. https://doi.org/10.1016/j.matlet.2018.02.031.
Song, K., Min, T., Seo, J., Ryu, S., Lee, H., Wang, Z., Choi, S.Y., Lee, J., Eom, C.B., Oh, S. H., 2021. Electronic and structural transitions of $LaAlO_3$/$SrTiO_3$ heterostructure driven by polar field-assisted oxygen vacancy formation at the surface. Adv. Sci. 8, 2002073. https://doi.org/10.1002/advs.202002073.
Thi, V.H.T., Lee, B.K., 2017. Effective photocatalytic degradation of paracetamol using La-doped ZnO photocatalyst under visible light irradiation. Mater. Res. Bull. 96, 171–182. https://doi.org/10.1016/j.materresbull.2017.04.028.
Van, P.V., Tuong, H.B., Tan, V.T., Thu, L.H., Khoang, N.D., Khiem, T.N., 2022. SnO_2/reduced graphene oxide nanocomposites for highly efficient photocatalytic

degradation of methylene blue. Opt. Mater. 123, 111916 https://doi.org/10.1016/j.optmat.2021.111916.

Vasiljevic, Z.Z., Dojcinovic, M.P., Vujancevic, J.D., Jankovic-Castvan, I., Ognjanovic, M., Tadic, N.B., 2020. Photocatalytic degradation of methylene blue under natural sunlight using iron titanate nanoparticles prepared by a modified sol-gel method. R. Soc. Open Sci. 7 (9), 200708 https://doi.org/10.1098/rsos.200708.

Yan, Z., Yang, X., Gao, G., Gao, R., Zhang, T., Tian, M., Su, H., Wang, S., 2022. Understanding of photocatalytic partial oxidation of methanol to methyl formate on surface doped La (Ce)-TiO_2: experiment and Dft calculation. SSRN Electron. J. 411, 31–40. https://doi.org/10.1016/j.jcat.2022.04.033.

Yayapao, O., Thongtem, T., Phuruangrat, A., Thongtem, S., 2015. Synthesis and characterization of highly efficient Gd doped ZnO photocatalyst irradiated with ultraviolet and visible radiations. Mater. Sci. Semicond. Process. 39, 786–792. https://doi.org/10.1016/j.mssp.2015.06.039.

Yu, F., Tian, F., Zou, H., Ye, Z., Peng, C., Huang, J., 2021. ZnO/biochar nanocomposites via solvent free ball milling for enhanced adsorption and photocatalytic degradation of methylene blue. J. Hazard. Mater. 415, 125511 https://doi.org/10.1016/j.jhazmat.2021.125511.

Zhou, W., Yu, B., Zhu, J., Li, K., 2022. Synthesis of ZnO/Ti_2C composites by electrostatic self-assembly for the photocatalytic degradation of methylene blue. J. Mater. Sci. 57, 1–17. https://doi.org/10.1007/s10853-021-06798-x.